Growth of ZnO:Al by atomic layer deposition: Deconvoluting the contribution of hydrogen interstitials and crystallographic texture on the conductivity

Ozhet Mauit[a], David Caffrey[b], Ardak Ainabayev[b,c], Aitkazy Kaisha[b], Olzat Toktarbaiuly[a], Yerzhigit Sugurbekov[a], Gulnar Sugurbekova[c], Igor V. Shvets[b], Karsten Fleischer[b,d]

[a]*National Laboratory Astana – Nazarbayev University, Astana, Kazakhstan*
[b]*School of physics and Centre for Research on Adaptive Nanostructures and Nanodevices (CRANN), Trinity College Dublin, Dublin 2, Ireland*
[c]*Nazarbayev University, Astana, Kazakhstan*
[d]*School of Physical Sciences, Dublin City University, Dublin 9, Ireland*

Abstract

Aluminium doped ZnO (AZO) is an interesting low cost transparent conducting oxide with further use as an inorganic transport layer in multilayer solar cells. Here we present our work on atomic layer deposited (ALD) thin films where, with optimised growth conditions, we can obtain resistivities of 1×10^{-3} Ωcm even in 50-80 nm thin films grown at low temperatures (250°C). We discuss the influence of crystallographic texture for ALD grown films by comparing plain glass, c-plane Al_2O_3, and a-plane Al_2O_3 substrates. We show that the doping mechanism in ALD grown AZO is more complex than for e.g. sputtered material as a substantial hydrogen interstitial related background doping occurs. We compare results from as grown samples with those briefly annealed at 320°C in nitrogen. This process leads to an increased Hall mobility due to improved grain boundary passivation, but reduced carrier concentration due to partial loss of hydrogen interstitials.

Keywords: Transparent Conducting Oxide, Atomic Layer Deposition, Aluminium doped Zinc Oxide, Hydrogen, Crystallographic Texture

1. Introduction

Transparent conducting oxides (TCOs) remain an important material class as front contacts for large area optoelectronic devices such as displays, thin film solar cells and smart windows [1–6]. One such material is Aluminium doped ZnO (AZO, ZnO:Al), which is of particular interest for low cost devices such as solar cells [7–9]. In order to achieve the required front contact sheet resistance of much less than 100 Ω/□, an AZO thickness of several hundreds nm is typically required. This poses a problem for many new low cost organic or halide perovskite solar cells, which typically use much thinner, smoother In_2O_3:Sn (ITO) or SnO_2:F (FTO) front contacts. However, ZnO and ZnO:Al are often used in the tunnelling contacts between consecutive cells in tandem solar cells, in particular in a-Si/μc-Si tandem cells [10–12]. In this case only very thin films are required, as the conduction band offset between absorbers and the ZnO/AZO is of larger importance to the cell's internal series resistance than the conductivity of the material. The concept of such ZnO based tunnelling contacts can also be used in organic and halide perovskite cells [13, 14], and there is growing interest in bulk hetero-junction cells based on organic/inorganic structures [15, 16]. For such structures the critical issue is to get high conductivities in thin TCO films (< 100 nm) at deposition temperatures compatible with the adjacent organic layers or plastic substrates.

One emerging deposition technique to obtain high quality, ultra-thin oxide layers is atomic layer deposition (ALD) [17–19]. Widely used for the growth of high quality gate oxides, such as Al_2O_3, ALD could become of increased interest in the field of TCOs. The inherently better performance of ALD grown TCOs, compared to nanoparticle assembled TCO layers, could make ALD attractive for thin film, and specifically low temperature processed tandem solar cells. In this work we therefore focus on the conductivities of thin ZnO:Al structures (50-80 nm) with an emphasis on the inherent transport properties in terms of scattering mechanism dependent on crystallographic texture, as well as the type of carrier generating defects. Using optimised procedures we are able to achieve good conductivities in very thin films, while maintaining a high electron mobility even at higher carrier concentrations.

2. Experimental details

Samples have been grown by atomic layer deposition (ALD, Model: Veeco Instruments, FijiTM G2 ALD) on a variety of substrates using diethyl-zinc (DEZ) as Zinc precursor, Trimethylaluminium as Al precursor, and water as oxidising agent. All ALD precursors have been supplied by Sigma Aldrich. The instruments base pressure was 2.5×10^{-4} Pa. High purity Argon (flow: 30 sccm) was used as carrier gas, N_2 was used as purging gas (flow: 100 sccm) to remove by-products. During purging the chamber pressure was at 41 Pa with peaks of 47-52 Pa during precursor deposition pulses. Super-cycles with varying

Email address: karsten.fleischer@dcu.ie (Karsten Fleischer)

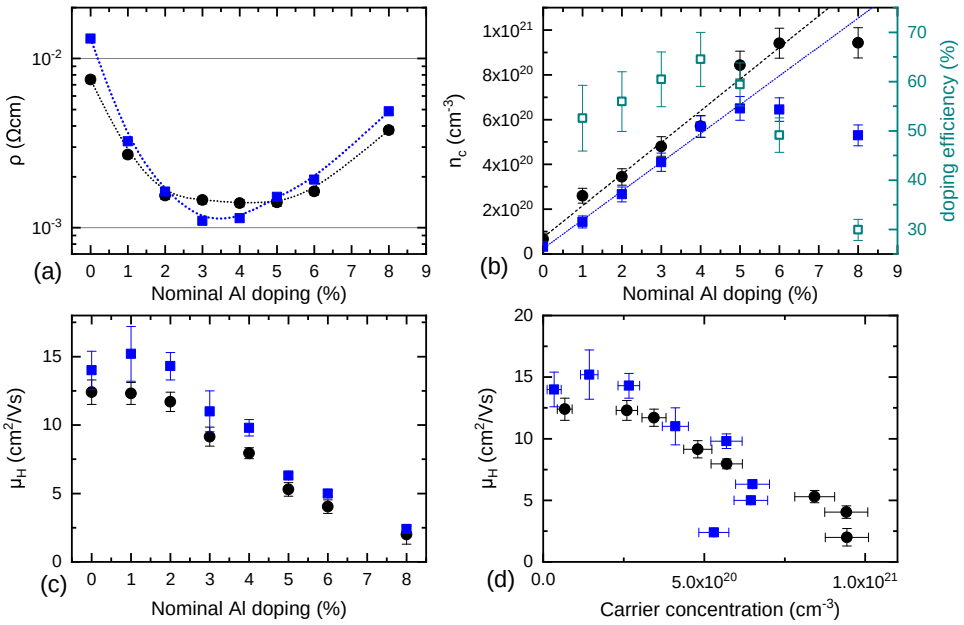

Figure 1: Overview of the electrical properties of ALD grown AZO on a-plane Al_2O_3 as function of nominal Al content. Data for as grown samples are indicated with (●), N_2 annealed samples with (■).
(a) Shows a broad minimum in resistivity between 2-5%, with N_2 annealed 3% samples showing the lowest overall resistivity. (b) The carrier concentration increases linearly with Al content up to 5%. We also show the doping efficiency for the annealed samples (□). (c) shows the Hall mobility, which decreases rapidly for samples with more than 2% Al content. (d) shows the Hall mobility as function of carrier concentration.

numbers of Al and Zn pulses have been used to vary the Al concentration. All substrates were initially treated to a water pulse (0.1 s). Afterwards, every metal precursor pulse (0.1 s) was followed by a water pulse (0.1 s) with a 10 s wait/purge step in-between. All pulse cycle times were chosen to be 40%-60% longer then previously determined saturation times for these precursors to ensure reproducible growth in a full saturation regime (Instrument manufacturer reference data). A sample thickness of ≈50 nm plain ZnO was achieved by 500 DEZ/H_2O-cycles on a-plane Al_2O_3. The ratio between Al and Zn pulses was increased, while keeping the number of total pulses as close to 500 as possible (e.g. 3% sample: [1 Al- every 32 Zn-pulses]$_{15}$ = 495 pulses). The substrate temperature during deposition was kept at 250°C, precursor lines were pre-heated to 150°C. The growth rate per cycle on a-plane sapphire (0.1 nm/cycle) was lower than under similar conditions on glass (0.16 nm/cycle). The latter is fully consistent with previous reports for films grown at 250°C [20]. The substrate dependent difference will be discussed below in terms of different crystallographic texture of the growing films.

The crystallographic properties of all films were analysed by X-ray diffraction (XRD) in symmetric $\theta/2\theta$ scans, as well as grazing incidence 2θ scans to analyse the predominant crystal orientation of the polycrystalline films. Both an Rigaku Smartlab Ultima IV and Bruker D8 Advance system using Cu Kα sources have been employed, the latter was equipped with a monochromized source using a Ge(002) double bounce monochromator. X-ray reflectivity (XRR) measurements were used to determine each individual samples thickness d to accurately calculate the film resistivity.

Electrical characterisation were done in a home built four point probe station using a square Van-der-Pauw geometry and silver paint based contacts. For Hall measurements a maximum field of 800 mT was used. The sample bias was kept between 10-20 mA with higher currents used for more conductive samples in order to maintain a comparable voltage drop over all samples. All electrical measurements were done using a Keithley 2400 source meter.

To investigate the influence of grain boundary scattering on the electron transport within the films all electrical measurements were performed before and after a brief nitrogen annealing cycle, where the sample temperature was increased to 320°C and immediately cooled down afterwards. The setup for this annealing procedure has been described elsewhere [21]. During the anneal only the sheet resistance is measured, using a linear arrangement of 4 gold plated, spring loaded contacts.

Normal incidence optical transmission and reflection measurements were performed in a PerkinElmer 650S UV-VIS spectrophotometer equipped with an integrating sphere.

3. Results

In line with previous work, the resistivity of the ALD grown ZnO films decreases with increasing Al content up to a nominal Al concentration of 3.5% [22–25]. Beyond that the carrier concentration continues to increase, saturating at 9×10^{20} cm^{-3}, though the decrease in electron mobility leads to an overall increase in resistivity. Figure 1 shows the resistivity, carrier concentration, and mobility as a function of nominal doping level, as well as the mobility as function of carrier concentration for polycrystalline films grown on a-plane sapphire. Both as-grown and N_2 annealed films are shown. For annealed films the doping efficiency was calculated assuming Al_{Zn} as the main dopant [19]. ALD grown AZO shows a much more complicated picture, compared to e.g. spray pyrolysis, or sputtered AZO:

- The low growth temperature, as well as the use of H_2O as oxidising agent leads to a substantial amount of hydrogen interstitials in addition to the Al substitutional doping. Nominally undoped ZnO therefore already shows a significant conductivity.

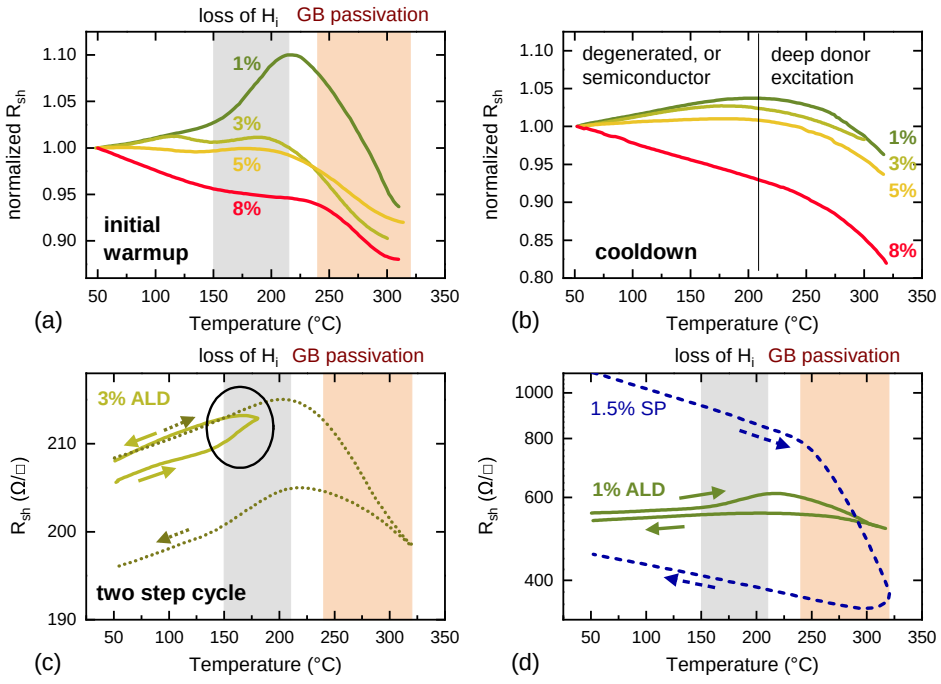

Figure 2: Normalised resistance versus temperature for 4 samples with varying Al content taken during initial heat up to 320°C (a) and during cool down (b). Normalised values are shown as the actual resistance varies significantly between samples. (c) shows the sheet resistance during a two step annealing cycle (50→180→50°C and 50→320→50°C) for a 3% sample. (d) compares the sheet resistance change of an ALD grown 1% sample during annealing to a 1.5% sample grown by spray pyrolysis at significantly higher temperatures (420°C)

- The crystallographic texture changes with increasing Al content (see below and e.g. [22]). In a bulk anisotropic, hexagonal material, a change of dominant crystalline orientation can alter the measured sheet resistance and hence the derived conductivity. While such changes are seen in other growth methods, mechanisms and magnitude differ in ALD grown films, as will be discussed below.
- In ALD grown films, the Al is not homogeneously distributed. Instead distinct high concentration Al layers have been observed by transmission electron microscopy [25–27]. Therefore ionised impurity scattering for isotropically distributed scattering sites can be mitigated leading to higher electron mobilities in highly doped films than e.g. seen in conventionally grown AZO [8, 28, 29].

In the following we will decouple these effects for our films by systematically comparing films with similar thickness, but different crystallographic texture as well as altering hydrogen content by post-annealing.

3.1. N_2 anneal – The contribution of H_i to σ:

In comparison to AZO grown by magnetron sputtering and spray pyrolysis, we notice stark differences during nitrogen anneal cycles up to 320°C. For conventional growth methods, increases in carrier mobility without significant changes in the carrier concentration are observed [21]. ALD grown samples instead show a consistent reduction in carrier concentration after the anneal of $\approx 1\times10^{20}\,\mathrm{cm}^{-3}$ for low Al doping concentrations. For the highest measured Al content an even higher carrier losses of up to $4\times10^{20}\,\mathrm{cm}^{-3}$ is found. As no significant changes in crystalline quality are seen in XRD measurements before and after annealing, it suggests that during the brief N_2 anneal the chemical environment of one carrier generating defect is altered. In the range of up to 5% Al content the loss in carrier concentration is entirely *independent* of the Al concentration. It has been noted, that for high Al concentrations the formation of AlO_x clusters can reduce doping efficiencies. Wu et al.[27] has shown that for high overall Al incorporation (>5%) Al diffusion into grain boundaries and AlO_x cluster formation leads to a decrease in doping efficiencies. This is consistent with the noticeable decline in carrier concentration and doping efficiencies for our films with more than 5% nominal Al content.

The loss in carrier concentration upon the brief N_2 anneal cycles however is inconsistent with a further migration of Al itself. In such a case the effect would scale with Al content, and show some onset threshold with Al concentration related to the solubility limit of Al within ZnO. In contrast, below 5% Al content, we observe a change independent of Al concentration. A similar reduction of $\approx 1\times10^{20}\,\mathrm{cm}^{-3}$ is even seen in nominally undoped samples, clearly indicating the involvement of a different doping mechanism.

We also observe a distinctly different resistance vs. temperature behaviour in such ALD grown films compared to spray pyrolysis or magnetron sputtered films (see Fig. 2d). Indeed, such samples show a significantly simpler behaviour during N_2 annealing and changes are dominated by grain boundary passivation at temperatures above 250°C [21, 30]. In sputtered, or SP grown films of similar dopant concentration no irreversible resistivity increases in the 150-210°C range are observed, the carrier concentration remains unchanged after full (320°C) annealing cycles, nor do we observe pronounced changes in the slope of resistance vs. temperature curves after the initial grain boundary passivation (see Fig. 2d). We therefore attribute the non-reversible resistivity increases in the 150-210°C range, only seen in ALD films, to the loss of a specific carrier (see black circle in Fig. 2c). The reversible change of slope above 220°C is

caused by the presence of deep donor levels in the more defective ALD grown material.

We thus conclude that the intentional, substitutional Al_{Zn} site is not affected. Instead another unintentional defect must be responsible. There has been an intensive discussion of whether oxygen vacancies, or hydrogen interstitials are the main unintentional n-type dopant in ZnO [31, 32]. Our results for ALD grown ZnO support the latter, as it is feasible that hydrogen interstitials can diffuse out of the thin films during the N_2 anneal, reducing the defect and therefore carrier concentration. In contrast oxygen vacancies would more likely form during annealing in oxygen free environments, hence an increase in carrier concentration would be expected in these circumstances. Figure 2(a) shows the normalised sheet resistance of a 1%, 3%, 5%, and 8% Al content sample during a heat cycle in nitrogen atmosphere. For heat treated samples (cool-down cycle) in the 50°C– 200°C range, the behaviour of all samples is consistent with degeneratively doped ZnO, where all carriers are already thermalized and increased phonon scattering leads to an increased resistivity at elevated temperatures. Only the 8% doped film shows a semiconducting behaviour, despite an even higher carrier concentration, illustrating the highly defective nature of such highly doped films. This suggests the high Al content already leads to significant modifications in the conduction band structure and thus energetic position of the dopant levels in addition to the already reported problems of dopant clustering [27].

At higher temperatures the excitation of carriers directly from deep donors (possibly V_O) to conduction band starts to dominate and the resistivity decreases. While this behaviour is expected for ZnO there are, as already discussed, significant deviations from this characteristic during the initial heat up in N_2 for the ALD-grown material. In particular there is an additional increase in resistivity in the region from 150°C–200°C most prominent for the lowest doped sample (here 1%, see Fig. 2(a)). We attribute this to a significant reduction in carrier concentration due to the loss of hydrogen interstitials (H_i). Figure 2(c) illustrates for a 3% sample, that this change is irreversible, and only seen in the initial heatup after growth. For higher Al concentration the overall behaviour is dominated by the substitutional doping and therefore the loss in H_i leads to less pronounced resistance changes in this temperature range. The behaviour is consistent with earlier first-principle studies, showing that significant H_i diffusion is expected above 125°C [33]. The ALD process, where water is used as an oxidizing agent, naturally is expected to have a higher hydrogen concentration compared to vacuum processed material. The larger loss in carrier concentration for films > 5% Al, suggests either a higher initial H_i concentration in the defective highly doped ZnO, or the onset of AlO_x clustering, leading to additional reduction in carrier concentration.

A second deviation from the stabilised resistance versus temperature curve occurs above 215°C, where the resistivity decreases dramatically again. The latter is seen more dramatically for spray pyrolysis grown material (Fig. 2(d)), and is linked to the passivation of grain boundaries, specifically the removal of charged oxygen species [21]. The behaviour of the ALD grown films is consistent with this. The effect being reduced at higher carrier concentrations and a higher carrier mobility being observed after annealing. (see Fig. 1).

3.2. The influence of Al content on crystalline texture

The hexagonal crystal structure in ZnO also leads to an anisotropy in the optical, and electrical properties of the material. Therefore the crystallographic texture of the thin film can also influence the films conductivity. Chemical vapour deposited, as well as magnetron sputtered ZnO often show preferred texturing with the growth direction being parallel to the c-axis of ZnO. During ALD growth the intermittent growth of AlO_x terminated surfaces can potentially affect the preferred growth direction. To investigate this we analysed the crystallographic texture as well as coherent crystal domain size for a set of different doping concentrations for films grown on a-plane Al_2O_3.

Figure 3 shows the XRD measurements of a set of samples with increasing Al content grown on a-plane Al_2O_3. Already in the raw data it is seen, that in addition to an expected shift in peak positions caused by the Al dopant induced strain, also the dominant growth direction is altered by the introduction of the Al. Peaks from (101) and (002) planes dominate with a change of dominant texture as function of doping level. The peak position gradually shift to higher angles, indicating a compression of the lattice spacing. In contrast to homogeneous, substitutional doping, the largest change in crystallographic texture is seen between the undoped samples and the smallest Al content. Undoped samples show a strong (101) plane expected for an epitaxial relationship of the ZnO with the a-plane sapphire. However, they also show a strong (002) reflex. The samples are therefore polycrystalline with a preferred a- and c-plane orientation of the individual crystals rather than being epitaxial. Upon introduction of the periodic AlO_x layers in small concentrations the system almost fully reverts to an a-plane orientation, with a dominant (101) reflex. Increasing the dopant concentration (and the internal strain), reverts the system back to an a-plane, c-plane mixed state, with a growing c-plane contribution. Up to a dopant concentration of 5% there is a fairly linear change of peak position (and $c-$axis lattice constant) with Al dopant content. For higher nominal doping levels this shift is stronger, indicating a higher rate of Al incorporation. A similar effect was previously seen in ALD AZO grown on quartz, where at a nominal 8% level the true Al content was found to be almost twice that much, while for 3% the true content was comparable to the nominal one [22]. In our case, based on the linear relationship of nominal Al content with carrier concentration and XRD peak position of up to 5%, we conclude a similar Al enrichment only occurs for higher doping levels, explaining the deterioration of crystalline quality as well as the significant reduction in doping efficiency above 5%.

A more detailed analysis of the XRD patterns reveals the detailed relationship of $a-$ and $c-$lattice parameter as well as the (110) texture coefficient with Al content (see Fig. 3(b,c)). The a- and c- axis were calculated from the measured positions of the (002), (101), (100) reflexes using the generic equation

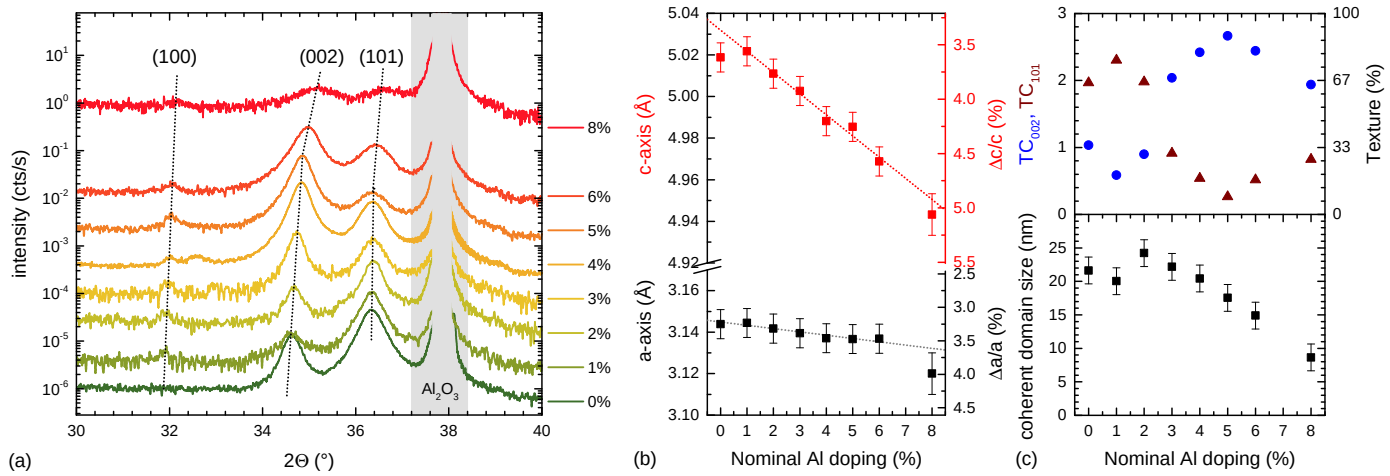

Figure 3: (a) X-ray diffractogram of AZO thin films grown on a-plane Al_2O_3 substrates. Data for different Al content have been stacked proportional to the Al content. (b) lattice parameter calculated from the (002) (c-axis), and (101), (100) (a-axis) reflex positions. (c) Texture coefficients for the 002 and 101 reflex (top) in absolute and relative values. Coherent domain size calculated via the Scherrer formula using the average value from the 002 and 101 reflex (bottom)

linking the d-spacing d of a given reflex with Miller index (hkl) to the lattice parameter a and c for a hexagonal crystal structure:

$$\frac{1}{d^2} = \frac{4}{3}\left(\frac{h^2 + hk + k^2}{a^2}\right) + \frac{l^2}{c^2}$$

The (002) reflex is solely linked to the $c-$lattice parameter, the (100) to the $a-$lattice parameter. As the (100) reflex is weak for most samples, a has also been calculated from the (101) position using c as determined from the (002) peak. The given value of a has been averaged between both methods, and the deviation used to approximate the error in determining the lattice constant. All ALD grown ZnO thin films, even in the undoped case, show a significant deviation from stoichiometric ZnO with both $a-$ and $c-$axis compressed by ≈3.5% compared to bulk ZnO due to the overall defective nature of the low temperature grown films. Analysis of the crystal structure of a 3% sample grown on a-plane sapphire from a corresponding grazing incidence measurement, reveals a similar lattice in-plane compression, ruling out any substrate induced uniaxial lattice distortion. A similar lattice compression has been observed in electrochemically altered ZnO nanoparticles where the effect was linked to the formation of oxygen vacancies [34].

For the doping range of 1% to 6% the $c-$axis further compresses linearly with the Al content, while only very small additional changes in $a-$ are observed. For higher concentrations of >6% we observe deviations from an expected linear behaviour, and deterioration of coherent domain size. This coincides with the increased hydrogen content in as-grown films above 5%. This raises the question if such highly cation doped films could see increased performance for hydrogen storage relative to more typically employed plain ZnO [35, 36]. The more defective nature of these highly doped films is also responsible for the observed limitations in Al doping efficiency and deterioration of conductive properties (see Fig. 1)

In this discussion we have, until now, implicitly excluded the thickness of the grown films. The measured sheet resistance and measured thickness from XRR was used to calculate the shown resistivities, eliminating the influence of differences in thickness onto the sheet resistance. As shown, there are significant changes in the crystalline orientation of the ZnO films upon increasing the Al content. As the ALD growth cycle is self saturating, assuming a constant fraction of surface atoms are used as adsorption sites for the precursors, a change in crystal orientation has a major impact on the observed growth rate. This is an expected consequence of the different surface atom density of different crystallographic planes. Indeed while the total number of cycles has been kept constant, the actual resulting film thickness did vary with Al content. The relationship between Al content and film thickness is however non-monotonic and therefore unrelated to an e.g. change of density (see Fig. 4). The overall behaviour is however very similar to the one of the texture coefficient TC_{002} (see Fig. 3). If we assume a strict linear relationship between growth rate and surface atom density one can understand the change in growth rate

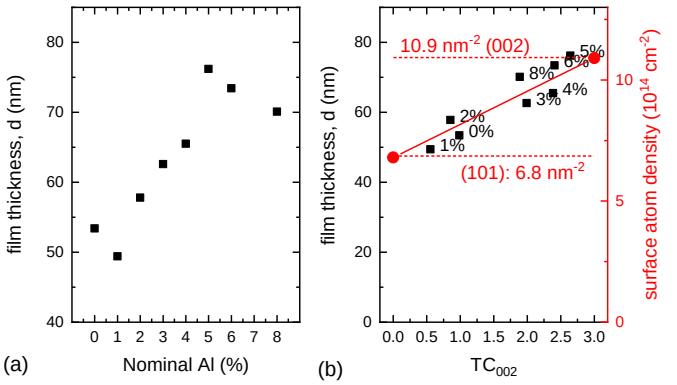

Figure 4: (a) Thickness of the ZnO films as function of nominal Al content. (b) Film thickness for the same films as function of the texture coefficient for the 002 (c-plane) oriented grains.

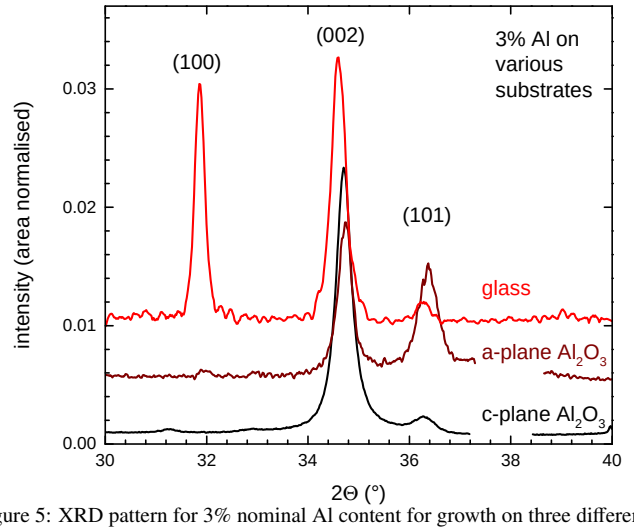

		a-plane, (GIXD)	c-plane	glass
c-axis	Å	5.00, (5.02)	5.01	5.02
a-axis	Å	3.14, (3.13)	3.22	3.15
TC_{002}		1.99, (0.93)	2.988	1.99
TC_{101}		0.95, (0.51)	0.008	0.05
TC_{100}		0.05, (1.56)	0.004	0.96
d_s	nm	22	22	33
d_{film}	nm	62	71	81
ρ	Ωcm	1.2×10^{-3}	8.4×10^{-4}	1.7×10^{-3}
μ_H	cm^2/Vs	12.4	12.7	13.3
n_c	cm^{-3}	4.0×10^{20}	5.7×10^{20}	2.6×10^{20}
R_s	Ω/□	220	120	220

Figure 5: XRD pattern for 3% nominal Al content for growth on three different substrates (a-, c-plane Al_2O_3, and glass). Measured data have been area normalised for better comparison and the area with a strong Al_2O_3 substrate signal was excluded. The adjacent table lists core sample properties of these samples including electrical properties after the N_2 anneal cycle. For comparison the crystallographic parameters and texture coefficient of the a-plane sample as determined by a grazing incidence X-ray diffraction (GIXD) measurement are also listed.

upon change of Al content, simply as a consequence of the altered surface texture. In Fig. 4 we plot the film thickness as function of Al content and texture factor. The straight line in Fig. 4 illustrates the expected change in surface atom density for a simple hexagonal lattice if one changes from 100% of the surface area being (101),(TC_{002} = 0) to 100% (002) oriented grains (TC_{002} = 3). The excellent agreement of the actual data for the samples grown on a-plane sapphire illustrates that variations in the film thickness in the ALD grown samples is not directly caused by e.g. density changes or non-stoichiometric Al inclusion, but are solely due to the change in dominant crystal orientation.

3.3. The influence of substrate induced texture

In order to evaluate if the change in crystallographic texture also directly influences the resistivity and carrier mobility we have investigated thin films of 3% doped ZnO grown simultaneously on various substrates (a-plane Al_2O_3, c-plane Al_2O_3, glass). The precursor cycle, temperature, total pressure etc. was therefore identical for all samples, yet crystallographic texture is expected to differ.

Figure 5 shows symmetric Θ/2Θ XRD scans of these samples, showing distinctly different texture. The film on c-plane Al_2O_3 has a strong (002) peak, indicating an almost exclusive crystal orientation where the ZnO c-axis is out-of plane (TC_{002} ≈ 3). For the sample grown on a-plane Al_2O_3 and glass there is still a preference for that orientation (TC_{002} ≈ 2). A distinct difference however is seen between the distribution of other crystal orientations. For the glass substrate, (100) is the second most frequent plane, while for the a-plane Al_2O_3 the it was the (101) reflex. As growth conditions were identical this behaviour must be caused by the initial nucleation on these substrates. It has been seen previously that ZnO crystalline orientation can vary between substrates in the case of Si and GaN [37].

As previously discussed, this change in texture is linked to the different film growth rates. Indeed for a set of 3% samples film thicknesses of 62, 71, and 81 nm were found for the simultaneously grown a-plane, c-plane Al_2O_3, and glass respectively. On the sapphire substrates, this is in line with the expectations of the change in surface atom density for the different orientations of a hexagonal unit cell (see Fig. 4). On the amorphous glass we observe an even higher growth rate, consistent with the model. One easy way to look at the growth rate as a function of film texture is the *d*-spacing of the actual reflex observed in XRD. Assuming no substantial differences in the adsorption probability for each individual Zn site (or OH group) for the different terminations, the precursor adsorption per cycle is proportional to the number of available sites. Consequently the number of cycles to complete a full ZnO plane remains similar for each plane. The growth rate is then also proportional to the $d-spacing$. The cycle normalised growth rate for the 3% doped ZnO on glass, c-plane Al_2O_3 and a-plane Al_2O_3 was found to be 1.62, 1.44, and 1.24 Å/cycle. The half values of the d-spacing of the (100), (002), and (101) reflexes of 1.40, 1.30, 1.24 Å respectively, closely follow the observed trend. The differences between substrates are a bit larger, as also surface morphology of the grains will have an effect.

Not surprisingly, the resistivities, mobilities, and carrier concentrations also vary with the substrate. The highest conductivity, mobility and carrier concentration was observed for the ZnO:Al grown on the c-plane Al_2O_3. As the sample grown on glass and a-plane Al_2O_3 show comparable properties, despite different crystal size and thickness, we conclude that these differences relate to the actual conductivity anisotropy of ZnO, or different barrier heights at grain boundaries depending on the relative orientation between adjacent grains. For the sample grown on c-plane Al_2O_3 the highest texture factor was observed, meaning there is a higher probability that neighbouring grains have the same orientation.

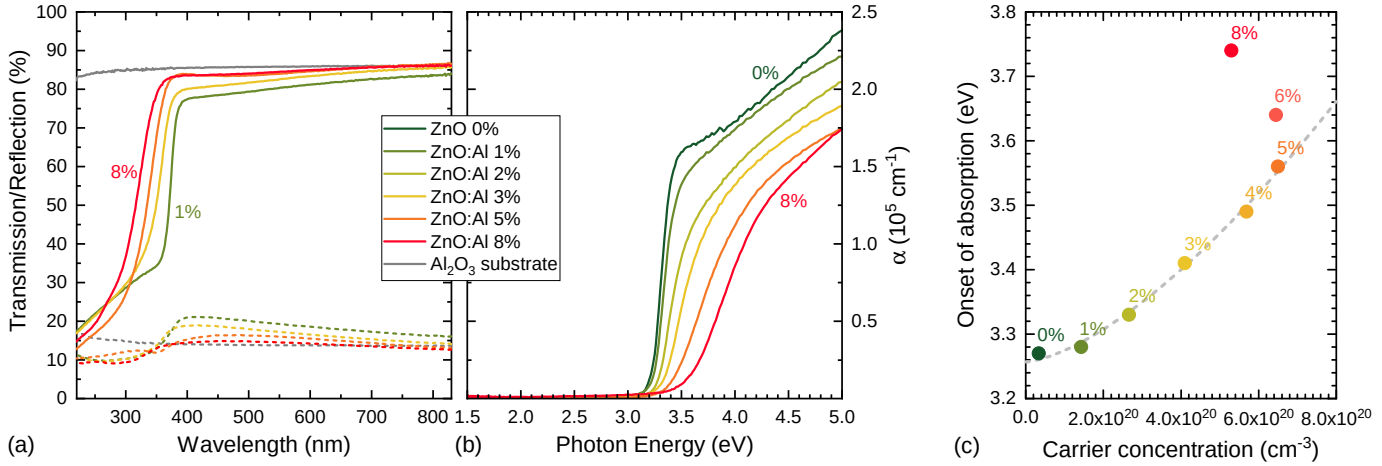

Figure 6: Optical measurements of ZnO:Al films grown on a-plane Al_2O_3. (a) compares the measured transmission (T) and reflectance (R) of thin films with the plain substrate (gray line). (b) shows the absorption coefficient, calculated from the T+R measurement. As the substrates absorption is negligable in the studied spectral range, this is therfore a direct measurement of α. (c) shows the onset of absorption as evaluated by Tauc-plots as function of the films carrier concentration. In the 0-5% doping region, the latter follows a power law with exponent 3/2 (dashed curve)

3.4. Optical properties

Given the intended use of the films as intermediate contact layers in solar cells, their optical properties are also of importance. Figure 6 summarises the transmission and reflectance measurements for the set of samples grown on a-plane Al_2O_3. Transmission is above 80% for the visible and near infrared range (see Fig. 6a). However, we stress that all changes in the raw transmission below the material's band gap are due to changes in reflectance of the entire stack of thin film and substrate. Such reflective losses will differ in full device structures, and can be even used to minimise overall reflectance of more comlex stacks [38], or help UV backreflection into top cells [39].

Analysing T+R data allows for the calculation of the absorption coefficent of the thin film itself [40, 41]. For these films, within the instrumental error, no actual absorption below the band gap is observed. Only the most defective sample (8%) shows residual defect related sub-gap absorption. Due to the high mobility, no free carrier absorption is observed within the accessible spectral range. Measurements before and after the brief N_2 anneal show no significant changes.

As visible light absorption does not change significantly, the observed changes in transmission can therefore be attributed to varying reflectance, primarily due to film thickness and crystallographic texture. ZnO is an anisotropic material with different refractive index and bandgap for light polarised along the c-axis ($n_{\parallel c}$) or perpendicular to it ($n_{\perp c}$) [42]. For unpolarised optical measurements in polycrystalline ZnO, we therefore have an effective medium with the overall refractive index depending on the ratios between $n_{\parallel c}$ and $n_{\perp c}$, which will depend on the texture coefficients

Likewise the observed increase in UV transmission by the expected blue shift upon doping, is not solely caused by the well known Burstein-Moss effect. Figure 6c shows the onset of optical absorption fitted by a Tauc plot as function of carrier concentration. The increase in the onset of absorption follows a power law with exponent 3/2 (dashed curve). For the Burstein-Moss effect an exponent of 2/3 would be expected, or an exponent of 1 if one includes effects due to ZnO's polar nature [43]. This discrepency clearly illustrates that other effects contribute in the case of ALD grown films. These include the texture change, size confinment due to the highly anisotropic nature of the dopant distribution, and for higher Al concentration (>6%) the amorphisation of the crystalline structure. As all these effects are intrinsically linked we can not seperate their individual contributions. The ALD grown samples show an overall stronger gap opening than expected for homogeneously doped films, and are hence good candidates for UV enhanced ZnO based front contacts.

4. Conclusion

We have shown that ALD growth of Al-doped ZnO at 250°C results in a highly conductive, fully transparent material well suited to for example being an intermediate contact layer in a variety of devices. The lowest observed resistivity was 8.5×10^{-4} Ωcm seen in only 70 nm thick layers grown on c-plane Al_2O_3.

By annealing of up to 320°C in an inert N_2 atmosphere, we were able to show that in ALD grown films, hydrogen significantly contributes to the conductivity in the low doping regime (< 1%). The films texture has a profound impact on film thickness (i.e. growth per ALD cycle) and varies for different substrates, and also Al concentrations. The root cause for the different textures are the initial nucleation processes depending on the substrate termination, and differences in Zn adsorption on Al terminated intermediate layers. It is therefore important when transferring growth processes from one substrate to another, or changing dopant concentration, to carefully check the growth rates and thin film orientation. Analysing the films texture by XRD gives an excellent tool to estimate the potential impact on the growth rate, as it is linked to the d-spacing of the dominant texture observed in symmetric XRD scans.

5. Acknowledgements

The authors would like to thank Science Foundation Ireland under grant no. 12/IA/1264, and SFI/12/RC/2278, as well as the support the Ministry of Education and Science of the Republic of Kazakhstan under Grant No. AP05134861 and 0115PK03029. Aitkazy Kaisha would like to acknowledge the support of the Kazakhstan government under the Bolashak program. Ainabayev Ardak gratefully acknowledge financial support of Nazarbayev University under the Talap program.

References

[1] W. Beyer, J. Hupkes, H. Stiebig, Transparent conducting oxide films for thin film silicon photovoltaics, Thin Solid Films 516 (2-4) (2007) 147–154.

[2] E. Fortunato, D. Ginley, H. Hosono, D. C. Paine, Transparent conducting oxides for photovoltaics, MRS Bull. 32 (3) (2007) 242–247.

[3] H. Hosono, H. Ohta, M. Orita, K. Ueda, M. Hirano, Frontier of transparent conductive oxide thin films, Vacuum 66 (3-4) (2002) 419–425.

[4] E. Fortunato, P. Barquinha, R. Martins, Oxide Semiconductor Thin-Film Transistors: A Review of Recent Advances, Adv. Mater. 24 (22) (2012) 2945–2986.

[5] C. Granqvist, Transparent conductors as solar energy materials: A panoramic review, Sol. Energy Mater. Sol. Cells 91 (17) (2007) 1529–1598.

[6] B. Szyszka, P. Loebmann, A. Georg, C. May, C. Elsaesser, Development of new transparent conductors and device applications utilizing a multidisciplinary approach, Thin Solid Films 518 (11) (2010) 3109–14.

[7] Ü. Özgür, Y. I. Alivov, C. Liu, A. Teke, M. Reshchikov, S. Doğan, V. Avrutin, S.-J. Cho, H. Morkoc, A comprehensive review of ZnO materials and devices, J. Appl. Phys. 98 (4) (2005) 041301.

[8] K. Ellmer, A. Bikowski, Intrinsic and extrinsic doping of ZnO and ZnO alloys, J. Phys. D: Appl. Phys. 49 (41) (2016) 413002.

[9] A. De Sio, K. Chakanga, O. Sergeev, K. Von Maydell, J. Parisi, E. Von Hauff, ITO-free inverted polymer solar cells with ZnO: Al cathodes and stable top anodes, Sol. Energy Mater. Sol. Cells 98 (2012) 52–56.

[10] J. Müller, B. Rech, J. Springer, M. Vanecek, TCO and light trapping in silicon thin film solar cells, Sol. Energy 77 (6) (2004) 917–930.

[11] D. Dominé, J. Bailat, J. Steinhauser, A. Shah, C. Ballif, Micromorph solar cell optimization using a ZnO layer as intermediate reflector, in: Photovoltaic Energy Conversion, Conference Record of the 2006 IEEE 4th World Conference on, Vol. 2, IEEE, 2006, pp. 1465–1468.

[12] S. Y. Myong, K. Sriprapha, S. Miyajima, M. Konagai, A. Yamada, High efficiency protocrystalline silicon/microcrystalline silicon tandem cell with zinc oxide intermediate layer, Appl. Phys. Lett. 90 (26).

[13] C.-H. Chou, W. L. Kwan, Z. Hong, L.-M. Chen, Y. Yang, A Metal-Oxide Interconnection Layer for Polymer Tandem Solar Cells with an Inverted Architecture, Adv. Mater. 23 (10) (2011) 1282+.

[14] Z. Yin, J. Wei, Q. Zheng, Interfacial Materials for Organic Solar Cells: Recent Advances and Perspectives, Adv. Sci. 3 (8).

[15] N. Aqab, H. Riaz, A. Nayfeh, Aluminum doped zinc oxide-silicon heterojunction solar cell by low temperature atomic layer deposition, in: IEEE 43rd Photovoltaic Specialists Conference (PVSC), 2016, p. 598.

[16] H. Saarenpää, T. Niemi, A. Tukiainen, H. Lemmetyinen, N. Tkachenko, Aluminum doped zinc oxide films grown by atomic layer deposition for organic photovoltaic devices, Sol. Energy Mater. Sol. Cells 94 (2010) 1379–1383.

[17] S. M. George, Atomic Layer Deposition: An Overview, Chem. Rev. 110 (2010) 111–131.

[18] M. D. Groner, F. H. Fabreguette, J. W. Elam, S. M. George, Low-Temperature Al2O3Atomic Layer Deposition, Chem. Mater. 16 (4) (2004) 639.

[19] A. Illiberi, R. Scherpenborg, Y. Wu, F. Roozeboom, P. Poodt, Spatial Atmospheric Atomic Layer Deposition of $Al_xZn_{1-x}O$, ACS Applied Materials & Interfaces 5 (24) (2013) 13124–13128.

[20] H. Beh, D. Hiller, M. Zacharias, Optimization of ALD-ZnO Thin Films Toward Higher Conductivity, physica status solidi (a) 215 (16) (2018) 1700880.

[21] D. Ali, M. Butt, C. Coughlan, D. Caffrey, I. Shvets, K. Fleischer, Nitrogen grain-boundary passivation of In-doped ZnO transparent conducting oxide, Phys. Rev. Mater. 2 (4) (2018) 043402.

[22] P. Banerjee, W.-J. Lee, K.-R. Bae, S. B. Lee, G. W. Rubloff, Structural, electrical, and optical properties of atomic layer deposition Al-doped ZnO films, J. Appl. Phys. 108 (2010) 043504.

[23] D.-J. Lee, H.-M. Kim, J.-Y. Kwon, H. Choi, S.-H. Kim, K.-B. Kim, Structural and Electrical Properties of Atomic Layer Deposited Al-Doped ZnO Films, Adv. Funct. Mater. 21 (3) (2011) 448–455.

[24] G. Luka, T. A. Krajewski, B. S. Witkowski, G. Wisz, I. S. Virt, E. Guziewicz, M. Godlewski, Aluminum-doped zinc oxide films grown by atomic layer deposition for transparent electrode applications, J Mater Sci: Mater Electron 22 (2011) 1810–1815.

[25] Y. Wu, P. Hermkens, B. Van de Loo, H. Knoops, S. Potts, M. Verheijen, F. Roozeboom, W. Kessels, Electrical transport and Al doping efficiency in nanoscale ZnO films prepared by atomic layer deposition, J. Appl. Phys. 114 (2) (2013) 024308.

[26] M. Verheijen, Y. Wu, D. Giddings, T. Prosa, D. Larson, F. Roozeboom, E. Kessels, Factors limiting the doping efficiency in atomic layer deposited ZnO:Al thin films: a dopant distribution study by transmission electron microscopy and atom probe tomography, in: European Microscopy Congress 2016: Proceedings, 2016, p. 888.

[27] Y. Wu, A. D. Giddings, M. A. Verheijen, B. Macco, T. J. Prosa, D. J. Larson, F. Roozeboom, W. M. M. Kessels, Dopant Distribution in Atomic Layer Deposited ZnO:Al Films Visualized by Transmission Electron Microscopy and Atom Probe Tomography, Chem. Mater. 30 (2018) 1209–1217.

[28] E. Arca, K. Fleischer, I. Shvets, Tuning the crystallographic, morphological, optical and electrical properties of ZnO: Al grown by spray pyrolysis, Thin Solid Films 555 (2014) 9–12.

[29] A. Bikowski, K. Ellmer, A comparative study of electronic and structural properties of polycrystalline and epitaxial magnetron-sputtered ZnO: Al and $Zn_{1-x}Mg_xO$:Al doped films. Origin of the grain barrier traps, J. Appl. Phys. 114 (6) (2013) 063709.

[30] D. Caffrey, E. Norton, C. O. Coileáin, C. M. Smith, B. Bulfin, L. Farrell, I. V. Shvets, K. Fleischer, Decoupling the refractive index from the electrical properties of transparent conducting oxides via periodic superlattices, Sci. Rep. 6 (2016) 33006.

[31] K. Ellmer, Past achievements and future challenges in the development of optically transparent electrodes, Nat. Photonics 6 (12) (2012) 809–817.

[32] C. Van de Walle, Hydrogen as a cause of doping in zinc oxide, Phys. Rev. Lett. 85 (5) (2000) 1012.

[33] J. Bang, K. J. Chang, Diffusion and thermal stability of hydrogen in ZnO, Appl. Phys. Lett. 92 (2008) 132109.

[34] S. A. Ansari, M. M. Khan, S. Kalathil, A. Nisar, J. Lee, M. H. Cho, Oxygen vacancy induced band gap narrowing of ZnO nanostructures by an electrochemically active biofilm, Nanoscale 5 (19) (2013) 9238–9246.

[35] M. Ahmad, R. ud Din, C. Pan, J. Zhu, Investigation of Hydrogen Storage Capabilities of ZnO-Based Nanostructures, J. Phys. Chem. C 114 (2010) 2560–2565.

[36] Z. Yaakob, D. J. Khadem, S. Shahgaldi, W. R. W. Daud, S. M. Tasirin, The role of Al and Mg in the hydrogen storage of electrospun ZnO nanofibers, Int. J. Hydrogen Energy 37 (2012) 8388–8394.

[37] Z. Baji, Z. Lábadi, Z. E. Horváth, I. Bársony, Structure and morphology of aluminium doped Zinc-oxide layers prepared by atomic layer deposition, Thin Solid Films 520 (2012) 4703–4706.

[38] K. Fleischer, E. Arca, I. Shvets, Improving solar cell efficiency with optically optimised TCO layers, Sol. Energy Mater. Sol. Cells 101 (2012) 262–269.

[39] A. Bielawny, C. Rockstuhl, F. Lederer, R. B. Wehrspohn, Intermediate reflectors for enhanced top cell performance in photovoltaic thin-film tandem cells, Opt. Express 17 (10) (2009) 8439–8446.

[40] L. Vriens, W. Rippens, Optical constants of absorbing thin solid films on a substrate, Applied optics 22 (24) (1983) 4105–4110.

[41] K. Fleischer, E. Norton, D. Mullarkey, D. Caffrey, I. Shvets, Quantifying the performance of p-type transparent conducting oxides by experimental methods, Materials 10 (9) (2017) 1019.

[42] G. E. Jellison, L. A. Boatner, Optical functions of uniaxial ZnO deter-

mined by generalized ellipsometry, Phys. Rev. B 58 (7) (1998) 3586–3589.

[43] B. E. Sernelius, K.-F. Berggren, Z.-C. Jin, I. Hamberg, C. G. Granqvist, Band-gap tailoring of ZnO by means of heavy Al doping, Physical Review B (17) (1988) 10244–10248.